10.1109/ULTSYM.2009.0151

Inducing Rapid Fluid Flows in Microchannels with Surface Acoustic Waves

Ming K. Tan, Leslie L. Yeo and James R. Friend
MicroNanophysics Research Laboratory
Monash University
Clayton, VIC, Australia

***Abstract*—We investigate uniform fluid and mixing flows with linear speeds up to 1–10 mm/s, actuated by surface acoustic waves. Under strong acoustic excitation, transition from uniform to oscillatory mixing flow occurs when the width of the channel increases beyond one acoustic wavelength of sound in the fluid λ_f. In this high velocity regime, particles of one micrometer in diameter suspended in aqueous solution are observed to follow the streamlines. Under weak acoustic excitation, particles aligning into equally-spaced lines (with a separation of $\lambda_f/2$) due to the presence of acoustic standing waves across the channel and move slowly in the reverse direction due to the slow streaming. We developed a numerical model of the system that accounts for the acoustic streaming in the fluid with treatment of viscous and solid-fluid coupling effects, and the results qualitatively support the observed phenomena in the experiments.**

I. Introduction

The dominance of surface tension and viscous forces at small scales greatly complicates efficient transport and mixing in microfluidic devices. In this paper, we elucidate the underlying mechanisms of phenomena peculiar to surface acoustic wave (SAW) excitation of fluids in microchannels—including the collection and transport of particles, and the appearance of vortices and concomitant mixing—with experimental observations and numerical modelling that incorporates spatial phase delay, viscous attenuation, and strong solid-fluid coupling effects unique to SAW excitation. The phenomenon are directly applicable to the sorting or patterning of particles in microchannels, and the switching between uniform flow for fluid delivery and vortex-laden flows for mixing in the same microchannel by simply changing the SAW frequency. This eliminates the typical requirements of elaborate architectures or separate components [1] to induce mixing. In addition, we demonstrate the ability to drive fluids in a microchannel at 1–10 mm/s—over one order of magnitude larger than current methods [2]—when the channel width is smaller than the SAW-induced sound wavelength in the fluid, i.e., $\mathcal{W}_{ch} < \lambda_f$.

The SAW used in this study is a *Rayleigh* wave [3]. It is generated by applying a sinusoidal electric potential to an interdigital transducer (IDT) on a piezoelectric substrate. While the SAW propagation on the substrate is confined to the x-axis from the transducer at a velocity of $v_{SAW} \approx 3990$ m/s, contact with a fluid medium through which sound propagates at speeds $c_0 < v_{SAW}$ ($c_0 \approx 1450$ m/s for water at ambient temperature) results in the radiation of acoustic energy from the substrate into the fluid at the Rayleigh angle $\theta_{SAW} = \sin^{-1}(c_0/v_{SAW})$ due to the vertical displacement of the substrate. If the substrate vibrates in a pure transverse mode (see Fig. 1(a)), sound wave is transmitted into the liquid at the Rayleigh angle. Over hundreds of oscillations of the substrate, this forms an (*Eckart* [4]) *acoustic streaming* force in the fluid due to the nonzero and temporally phase-shifted distribution of the pressure and velocity [5], [6]. Eckart streaming is a *far-field* streaming and the length scale of the fluid motion is larger than the acoustic wavelength, $\mathfrak{L}_f > \lambda_f$. On the other hand, if the substrate vibrates in pure compressional mode (see Fig. 1(b)), a thin shear viscous boundary layer is generated due to the high shear attenuation of the liquid to resist any shear motion. The thickness of this viscous boundary layer is [7]

$$\delta_v \equiv \sqrt{\frac{2\mu}{\rho_f \omega}}, \tag{1}$$

where μ is the fluid viscosity and ω is the angular frequency. Again, over hundreds of oscillations, this high shear viscous absorption layer adjacent to the free surface of the vibrating substrate gives rise to *boundary layer streaming* [5], [6], [8], which is confined to a thin viscous boundary layer in contrast to Eckart streaming. Boundary layer streaming is a *near-field* streaming and the length scale of the fluid motion is smaller than the acoustic wavelength, $\mathfrak{L}_f < \lambda_f$. Acoustic streaming has been exploited in droplet transport [9], microjet [10], chaotic convection [11], and microparticle concentration [12] under simpler excitation conditions than used here, where all of these effects are significant and combine with direct acoustic forces on the particles suspended in the fluid [13] to give rise to the

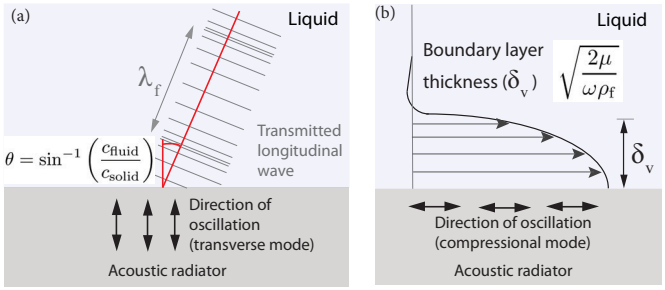

Fig. 1. Transmission of sound from a solid substrate (acoustic radiator) into a fluid when (a) a pure transverse wave and (b) a pure compressional wave propagates in the solid.

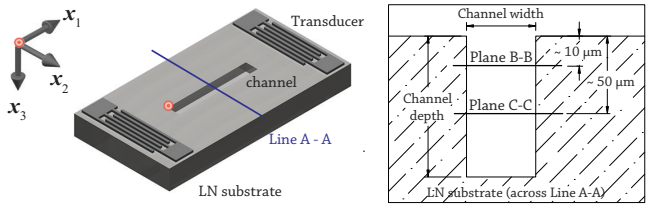

Fig. 2. The cut channel and the different viewing planes where the experimental images were acquired. The dot at the corner of the channel indicates the origin of the coordinates: x_1 lies along the channel length $\mathcal{L}_{\rm ch}$, x_2 is along the channel width $\mathcal{W}_{\rm ch}$, and x_3 points into the substrate along the channel depth $\mathcal{D}_{\rm ch}$.

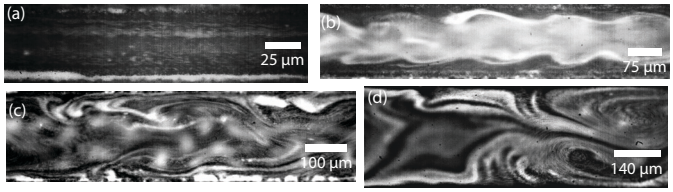

Fig. 3. Images (a)–(d) showing typical flow behavior along plane B–B in $\mathcal{W}_{\rm ch} = 50$, 150, 200, and 280 μm wide microchannels when driven by 20 MHz SAW.

phenomena described in this paper.

II. Experimental Method and Results

Standard photolithography was used to fabricate a collection of 20 MHz and 30 MHz SAW devices using 127.68°-rotated Y-cut X-propagating single-crystal LN. We then cut rectangular microchannels $\mathcal{L}_{\rm ch} = 10$ mm long and $\mathcal{D}_{\rm ch} = 180$ μm deep with widths of $\mathcal{W}_{\rm ch} = 30$, 50, 150, 200 and 280 μm into the LN substrates of devices designed to operate at 20 and 30 MHz using a KrF 248 nm exciplex laser (Extech Ltd., Oxford, England) as shown in Fig. 2; the SAW wavelength $\lambda_{\rm SAW}$ is approximately 200 μm and 133 μm, respectively. The microchannel was then filled with a deionized aqueous, homogeneous suspension of $\phi_{\rm p} = 500$ nm and 1 μm diameter spherical fluorescent polystyrene particles (BioScientific, Gymea NSW) selected to ensure that $\phi_{\rm p} \ll \lambda_{\rm f}$ and $\phi_{\rm p} \ll \mathcal{W}_{\rm ch}$. At room temperature, $\lambda_{\rm f} \approx 73$ and 48 μm for the 20 MHz and 30 MHz sound waves in water, respectively. The different planes in Fig. 2 are sections along the channel where experimental observations were made. A damping material (α-gel, Geltec Ltd., Yokohama, Japan) was used to minimize wave reflection from the substrate ends.

A sinusoidal electrical signal was applied to the input IDT at a frequency matching the IDT resonance. Along plane B–B, uniform fluid flow is observed at approximately 3.5 mm/s in the same direction as the SAW along the channel in a 50 μm wide channel (Fig. 3(a)) when the SAW device is driven continuously at 20 MHz and 400 mW. The flow was observed using microscopic flow visualization (BXFM stereomicroscope and iSpeed camera, Olympus, Japan) at 60 frames/second. Holding the input power constant at 400 mW, as the width of the channel in the 20 MHz device is increased from $\mathcal{W}_{\rm ch} = 150$ to 200 and 280 μm, the flow becomes progressively more irregular as shown in Figs. 3(b)–(d). Similarly, uniform flow transitions to mixing for the 30 MHz device when $\mathcal{W}_{\rm ch}$ increases beyond 30 μm. For both cases, flow irregularities appear when $\mathcal{W}_{\rm ch} > \lambda_{\rm f}$. However, at plane C–C and deeper in the channel the flow velocity is reduced and particles collect along equally-spaced lines roughly parallel to the x-axis, as shown in Figs. 4(a)–(b). These collected particles actually move along the lines in a direction *opposing* the propagation direction of the SAW (Figs. 4(d)–(f)) at a speed of approximately 0.1 mm/s. We note here that at a constant input power to the transducer, flows at plane B–B is excited with a high amplitude vibration whereas the flows at plane C–C is excited with a the low amplitude vibration.

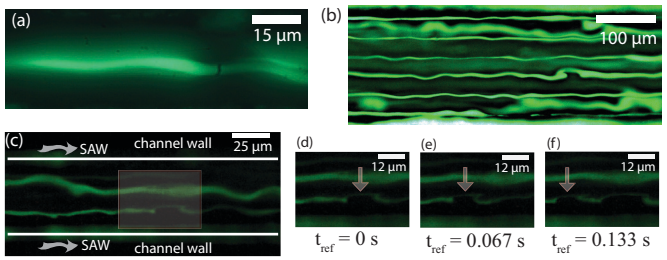

Fig. 4. The behavior along plane C–C is rather different: 500 nm particles collect into either one or six lines in a (a) 30 μm or (b) 200 μm wide channel, respectively, under 30 MHz SAW excitation. Experimental image (c) showing the accumulation of 500 nm particles at the nodes of the pressure field in a 150 μm wide channel. These collected particles appear to be moving from right to left along the nodal lines opposite the SAW propagating from left to right, as shown in the magnification of a section in the channel in (d, e, f).

III. Numerical Model

To analyze the problem, a two-dimensional numerical model of the phenomena was constructed for the x_1–x_2 plane in Fig. 2, including linear piezoelectric coupling equations [14], the first-order Navier-Stokes equation [7] with acoustic streaming equations [5] to accommodate the time-averaged fluid flow arising from the SAW irradiation, viscous effects, and the effect of attenuation in the SAW propagation as a consequence of the fluid present in the channel. The method of the analysis has been reported in [15].

IV. Numerical Results and Discussions

A. First order sound field

Given that the two sidewalls of the microchannel at $x_2 = 0, \mathcal{W}_{\rm ch}$ act as parallel radiators, the transmitted acoustic waves superimpose to form a transverse standing wave across the channel width. Figure 5(a) shows the corresponding solution for the first-order fluid pressure field in the 280 μm wide channel at the end of the 200th cycle. Also shown are 500 nm particles as they collect along lines in plane C–C (Fig. 5(b)); the separation between the particle collection lines is approximately 36 μm for the 20 MHz device and 24 μm for a 30 MHz device (not shown), corresponding to $\lambda_{\rm f}/2$. A comparison (Fig. 5(c)) between the numerical and experimental results suggests 500 nm particles are trapped at the nodes of the pressure field: a 280 μm wide channel under

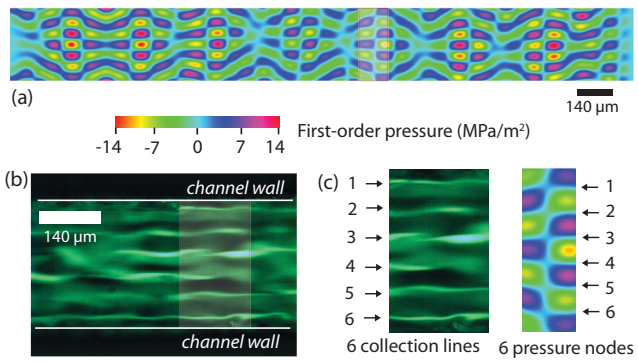

Fig. 5. The calculated (a) first-order pressure distribution in the fluid in a 280 μm wide channel shows the standing wave formed by cross-channel interference between waves propagating from either side of the channel after 200 cycles ($t \approx 10$ μs). Experimental image (b) showing the collection of 500 nm particles at matching locations across the 280 μm channel along plane C–C when driven by 20 MHz SAW. Comparison (c) between the numerical and experimental results indicate that the particles collect along the nodes of the pressure field.

20 MHz SAW excitation forms six lines of particles aligned to the quiescent regions in the pressure field in the fluid. We note here $\rho_{\rm p}$ (≈ 1050 kg/m^3) $> \rho_{\rm f}$, consistent with the literature that particle denser than the liquid should toward the pressure nodes [16], [17]. Similar behavior is observed if the 1 μm particles are used. The number of collection lines is an integer number of nodal lines with separation $\lambda_{\rm f}/2$ that fit within the given channel width, consistent with past studies [18], [19] and our results in Fig. 4(a–b).

B. Second order streaming field

By applying 1 $V_{\rm p-p}$ on the transducer, the calculated streaming velocity field shows the flow is in the reverse direction from downstream to upstream of the channel, as shown in Fig. 6(a). The reverse flow is related to the retrograde motion of the solid elements on the channel walls. The large acceleration of these elements gives rise to a large streaming force in the x_1-direction within the viscous boundary layer of thickness $\delta_v \sim \mathcal{O}(10^{-7})$ m adjacent to the wall due to the large dissipative effects there, as shown by the sharp increase in $u_{\rm dc}$ near the wall in Figs. 6(d) and (f). Consequently, strong clockwise vortical flow arises in the boundary layer as illustrated in Fig. 6(a). Since the large inertial effects decays away from the wall into the fluid, a net flow, however, results in the boundary layer in the direction *opposing* the SAW propagation. These vortices generate a time-averaged inertial force in the bulk of the fluid.

Closer examination of the particle "lines" exposes serpentine-like undulations of particle trajectories in Figs. 4(d)–(f), and in conjunction with the numerical result in Fig. 6(a), we speculate that these suspended particles in aqueous solution are subjected to two strong forces: acoustic radiation force and streaming drag force. The motion of these particles is restricted by the first-order standing wave field, where these particles are accumulated at the pressure

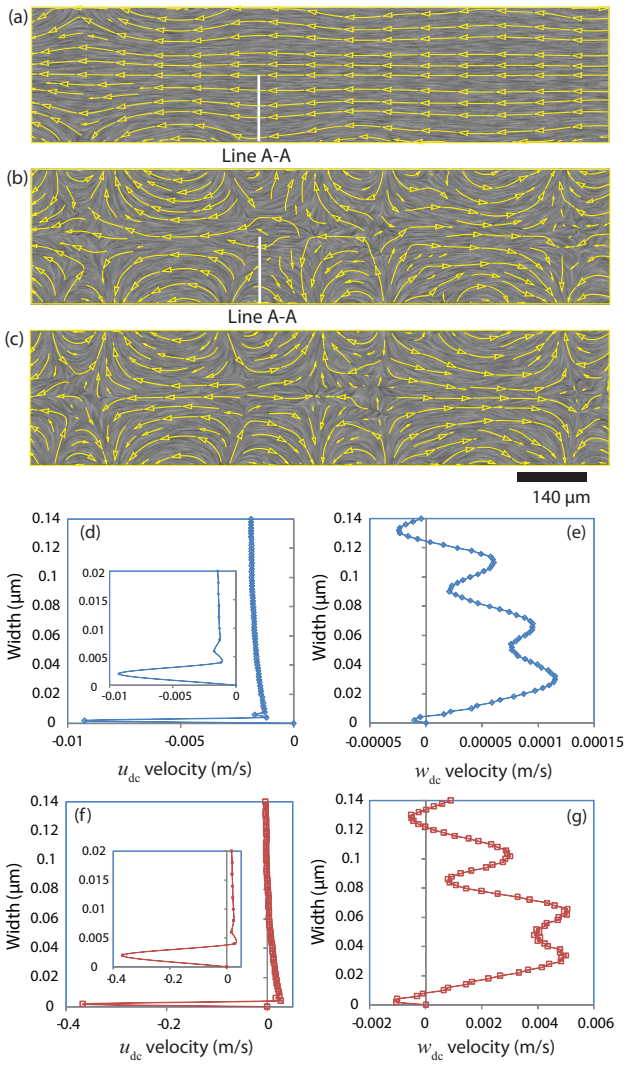

Fig. 6. Streamline plot of the acoustic streaming velocity field $\mathbf{u}_{\rm dc}$ in the 280 μm wide channel when the transducer on the solid substrate is driven at (a) 1 $V_{\rm p-p}$, (b) 10 $V_{\rm p-p}$, and (c) 20 $V_{\rm p-p}$—representing low, mid and high power—for a duration of 10 μs (200 cycles). The $u_{\rm dc}$ velocity amplitude under low, mid and high power are $\mathcal{O}(10^{-2})$ m/s, $\mathcal{O}(1)$ m/s and $\mathcal{O}(1)$ m/s, respectively, whereas for the $w_{\rm dc}$ velocity amplitude are $\mathcal{O}(10^{-3})$ m/s, $\mathcal{O}(10^{-1})$ m/s and $\mathcal{O}(10^{-1})$ m/s, respectively. The $u_{\rm dc}$ and $w_{\rm dc}$ velocity profiles along the line A-A are shown in (d, e) for low power, and (f, g) for mid power. Finer details of the abrupt increase in the fluid velocity near the wall due to the boundary layer streaming is shown in the inset in (d) and (f).

nodal lines and drag by the acoustic streaming to move in the reverse direction.

The vortical flow across the entire channel begins to emerge once the applied voltage is increased to 10 $V_{\rm p-p}$ and intensifies further at 20 $V_{\rm p-p}$, as shown in Figs. 6(b) and (c) for the 280 μm channel. Examination of the plots in Figs. 6(d) and (e) reveals that the increase in the velocity parallel to the channel walls $u_{\rm dc}$, upon increasing the electrical potential from 1 $V_{\rm p-p}$ to 10 $V_{\rm p-p}$, is mostly confined within the thin boundary layer δ_v, whereas the transverse velocity $w_{\rm dc}$ increases throughout the entire channel width. This strongly suggests that by increasing the power, the unidirectional flow

field as observed in low power regime (see Fig. 6(a)) break down as a result of the high transverse velocity $w_{\rm dc}$ across the width of the channel, giving rise to a large torque that, in turn, gives rise to vortical flow shown in Figs. 6(b) and (c), consistent with the experimental result as shown in Fig. 3(d).

By comparing the displacement amplitude of the solid element on the channel wall $\zeta_{\rm s}$ and the boundary layer thickness δ_v, we observe that $\zeta_{\rm s}/\delta_v < 1$ for the high power regime, $\zeta_{\rm s}/\delta_v \ll 1$ for the low power regime, suggesting that the streaming outside the boundary layer becomes stronger when the displacement amplitude of the solid element becomes comparable to the thickness of the boundary layer. Therefore, the flow is dominated by boundary layer streaming in low power regime, and shifts to Eckart streaming at high power regime provided that $\mathcal{W}_{\rm ch} \approx \mathfrak{L}_{\rm f} > \lambda_{\rm f}$, which ensures a sufficient distance from the acoustic radiator for the Eckart streaming force to buildup. This is interesting since we have seen from the experimental results that the flow transition from uniform unidirectional flow to vortical flow also depends on the channel width (see Fig. 3); uniform and unidirectional flow occurs when $\mathcal{W}_{\rm ch} < \lambda_{\rm f}$ (dominated by near-field streaming) and vortical flow when $\mathcal{W}_{\rm ch} > \lambda_{\rm f}$ (dominated by far-field streaming). Clearly, for acoustic streaming in narrow channels ($\delta_v < \mathcal{W}_{\rm ch} < \lambda_{\rm f}$), the flow in the bulk of the fluid is the result of the boundary layer streaming.

Experiments conducted by Cecchini *et al.* [20], [21] on water entry into a microchannel fabricated on 160 MHz SAW device exhibited a similar *counterflow* behavior where the water flows in the direction opposite to the propagating SAW. Based on their experimental observations, the authors concluded that the driving mechanism is due to the SAW-assisted coalescence. In their experiment setup, $\lambda_{\rm f} \approx 9.3$ μm and the channel heights $\mathcal{H}_{\rm ch}$ is between 10 and 50 μm and thus $\mathcal{H}_{\rm ch} > \lambda_{\rm f}$. We note here that the channel width $\mathcal{W}_{\rm ch}$ defined in our experiment is equivalent to the channel height in their experiment $\mathcal{H}_{\rm ch}$, which refers to the transverse direction. They observed that counterflow occurs in the low power regime, similar to the case we have presented for the opposite flow in 280 μm wide channel ($\mathcal{W}_{\rm ch} > \lambda_{\rm f}$) under low amplitude vibration ($\zeta_{\rm s}/\delta_v \ll 1$). In the high power regime, they observed that water flows in the same direction as the travelling SAW, suggesting that the flow is dominated by Eckart streaming ($\mathcal{H}_{\rm ch} > \lambda_{\rm f}$).

V. Conclusion

Our two-dimensional model is sufficient to describe the salient features of the experimentally observed flow even with the free surface along the top of the fluid channel absent in the numerical treatment. The numerical result agreed with the experimental results qualitatively and the constructed numerical model is able to elucidate the physics behind this particle collection across the channel width and the flow transition from the uniform and unidirectional flow at the low power regime into the vortical flow at the high power regime.

Acknowledgment

The authors thank Professor Omar K. Matar for help with the solving of the fluid second-order equations using LSODE and for pointing out the importance of using the empirical equation of state to take into account the nonlinear parameter. His suggestions have led to significant improvements to this work.

References

[1] H. Stone, A. Stroock, and A. Ajdari, "Engineering flows in small devices: microfluidics towards a lab-on-a-chip," *Annu. Rev. Fluid Mech.*, vol. 36, pp. 381–411, 2004.

[2] D. Laser and J. Santiago, "A review of micropumps," *J. Micromech. Microeng.*, vol. 14, pp. R35–R64, 2004.

[3] R. White and F. Voltmer, "Direct piezoelectric coupling to surface elastic waves," *Appl. Phys. Lett.*, vol. 7, pp. 314–316, 1965.

[4] C. Eckart, "Vortices and streams caused by sound waves," *Phys. Rev.*, vol. 73, pp. 68–76, 1948.

[5] C. Bradley, "Acoustic streaming field structure: The influence of the radiator," *J. Acoust. Soc. Am.*, vol. 100, no. 3, pp. 1399–1408, 1996.

[6] L. D. Rozenberg, *High-Intensity Ultrasonic Fields*. Plenum Press., 1971.

[7] P. Morse and K. Ingard, *Theoretical Acoustics*. MacGraw-Hill, 1968.

[8] H. Schlichting, *Boundary Layer Theory*. McGraw-Hill, Inc, 1968.

[9] M. Tan, J. Friend, and L. Yeo, "Microparticle collection and concentration via a miniature surface acoustic wave deivce," *Lab Chip*, vol. 7, pp. 618–625, 2007.

[10] M. K. Tan, J. R. Friend, and Y. Y. Leslie, "Interacial jetting phenomena induced by focused surface vibrations," *Phys. Rev. Lett.*, vol. 103, p. 024501, 2009.

[11] T. Frommelt, M. Kostur, M. Schäfer, P. Talkner, P. Hänggi, and A. Wixforth, "Microfluidic mixing via acoustically driven chaotic advection," *Phys. Rev. Lett.*, vol. 100, p. 034502, 2008.

[12] H. Li, J. Friend, and L. Yeo, "Surface acoustic wave concentration of particle and bioparticle suspension," *Biomed. Microdevices*, vol. 9, pp. 647–656, 2007.

[13] N. Aboobaker, D. Blackmore, and J. Meegoda, "Mathematical modeling of the movement of suspended particles subjected to acoustic and flow fields," *Appl. Math. Model.*, vol. 29, no. 6, pp. 515–532, 2005.

[14] B. Auld, *Acoustic Fields and Waves in Solids*. Wiley, 1973, vol. 1 and 2.

[15] M. K. Tan, Y. Y. Leslie, and J. R. Friend, "Rapid fluid flow and mixing induced in microchannels using surface acoustic waves," *EPL*, vol. 87, p. 47003, 2009.

[16] L. King, "On the Acoustic Radiation Pressure on Spheres," *Proc. Roy. Soc. Lond. Math. Phys. Sci.*, vol. 147, no. 861, pp. 212–240, 1934.

[17] A. A. Doinikov, "Theory of acoustic radiation pressure for actual fluids," *Phys. Rev. E*, vol. 54, pp. 6297–6303, 1996.

[18] P. Vainshtein, M. Fichman, K. Shuster, and C. Gutfinger, "The effect of centerline particle concentration in a wave tube," *J. Fluid Mech.*, vol. 306, pp. 31–42, 1996.

[19] J. Spengler, W. Coakley, and K. Christensen, "Microstreaming effects on particle concentration in an ultrasonic standing wave," *AIChE J.*, vol. 49, no. 11, pp. 2773–2782, 2003.

[20] M. Cecchini, S. Girardo, D. Pisignano, R. Cingolani, and F. Beltram, "Acoustic-counterflow microfluidics by surface acoustic waves," *Appl. Phys. Lett.*, vol. 92, p. 104103, 2008.

[21] S. Girardo, M. Cecchini, F. Beltram, R. Cingolani, and D. Pisignano, "Polydimethylsiloxane-$LiNbO_3$ surface acoustic wave micropump devices for fluid control into microchannels," *Lab Chip*, vol. 8, pp. 1557–1563, 2008.